ACS APPLIED NANO MATERIALS
Cite This: ACS Appl. Nano Mater. 2019, 2, 2533−2541
Article
www.acsanm.org

Nanoparticle-Assembled Gold Microtubes Built on Fungi Templates for SERS-Based Molecular Sensing

Umapada Pal,*[,†] Dulce Natalia Castillo López,[†,‡] Moisés Graciano Carcaño-Montiel,[§] Lucía López-Reyes,[§] Pablo Díaz-Nuñez,[⊥] and Ovidio Peña-Rodríguez[⊥]

[†]Instituto de Física, Benemérita Universidad Autónoma de Puebla, Apartado Postal J-48, Puebla 72570, Mexico
[§]Laboratorio de Microbiología de Suelos, Centro de Investigación en Ciencias Microbiológicas, ICUAP, Benemérita Universidad Autónoma de Puebla,Puebla 72570, Mexico
[⊥]Instituto de Fusión Nuclear, Universidad Politécnica de Madrid, C/José Gutiérrez Abascal 2, Madrid E-28006, Spain

Supporting Information

ABSTRACT: Development of highly sensitive molecular sensors is of immense current interest for biomedical diagnosis. Although the possibility of single molecule detection through plasmonic sensors based on surface enhanced Raman scattering (SERS) has been demonstrated, the practical application of such devices is hindered due their complex fabrication strategies and inhomogeneous Raman signal response. Here we present a simple biological method for large scale fabrication of plasmonic microtubes using selective nonpathogenic fungi as living templates. The biologically fabricated microstructures can be used as SERS substrates for the detection of organic molecules with signal enhancement factors as high as 1×10^{10}, exploiting their rugged, highly porous surfaces with intense hot spots. Although they are structurally not as perfect as those of chemically or physically fabricated plasmonic SERS substrates, their morphological/geometrical inhomogeneity introduces only about a one order fluctuation of SERS enhancement factor along their lengths. The plasmonic microstructures have great potential for the fabrication of cheap, efficient, and highly sensitive gold-based biosensors for the detection and monitoring of organic molecules.

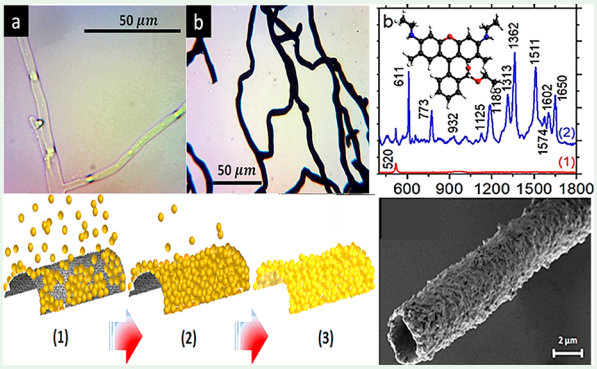

KEYWORDS: *plasmonic microtubes, fungal biotemplate, surface-enhanced spectroscopy, molecular sensing*

INTRODUCTION

With the progress of plasmonics, specifically the advancements in techniques for fabricating size- and shape-controlled plasmonic nanostructures, the sensitivity of molecular detection has improved substantially in recent times.[1−8] The most sensitive technique known for detecting organic molecules is surface-enhanced Raman scattering (SERS),[9] for which self-assembled plasmonic nanostructures are frequently utilized as substrates or supports for analyte molecules. A chemically or physically engineered assembly of plasmonic nanostructures produces inhomogeneous electric field distribution, concentrating the electric field at "hot spots", usually located at interparticle spaces. On excitation in resonance or close to the frequency of surface plasmon (SP) of the assembled plasmonic nanostructures, the high electric field (near-electric field) enhances the Raman signals of analytes physically or chemically attached to the substrate.[10] In fact, the sensitivity of a molecular sensor depends both on the quality of SERS substrate and the nature of the adsorbed analyte,[11] apart from the nature (wavelength and intensity) of excitation used for generating the Raman signal.[12] Although a substantial progress has been made on the optimization of the latter two parameters, fabrication of efficient substrates to generate optimum SERS signal is an area that needs further attention for the development of efficient SERS-based molecular sensors. Controlled fabrication of homogeneous SERS substrates on a large scale is indispensable to fulfill the envisioned merits of such devices and their practical applications.

Among the frequently used physical and chemical techniques such as electron beam lithography and nanotransfer printing,[13,14] chemically coordinated self-assembly or surface immobilization,[15,16] template-assisted assembly,[17,18] etc., physical and template-assisted electrochemical techniques can produce plasmonic SERS substrates with signal enhancement factors (EFs)[18,19] as high as 1×10^7. On the other hand, using chemical or chemically coordinated techniques, SERS substrates could be fabricated with EFs high enough for single-molecule detection.[20] Although plasmonic substrates with excellent SERS performance could be fabricated using the selective physical and chemical techniques mentioned above,

Received: March 8, 2019
Accepted: April 5, 2019
Published: April 5, 2019

DOI: 10.1021/acsanm.9b00443
ACS Appl. Nano Mater. 2019, 2, 2533−2541

most of them involve complicated, expensive, and non-environmentally friendly processes.[21,22]

On the other hand, several self-assembled plasmonic nano- and microstructures have been fabricated through biological routes,[23−31] although they have rarely been tested as SERS substrates. Among the few reports of using biotemplated plasmonic structures in SERS, the most significant one is the fabrication of Au microspheres using bacterial spores by Yang et al.,[32] achieving SERS signal EF as high as 1×10^{11}. Considering the fabrication complexity of SERS substrates through conventional physical and chemical processes, biological techniques seem to be one of the most promising ones because of their simplicity, cost effectiveness, and environmentally benign natures.

Here we report a simple, green technique for the fabrication of Au microtubes, utilizing living nonpathogenic tubular fungi such as *Trichoderma asperellum* (*T. asperellum*) and *Aspergillus sydowii* (*A. sydowii*). We demonstrate that these rugged gold microtubes are excellent SERS substrates, which can be used to detect organic molecules dissolved in water in concentrations as low as 1×10^{-9} M. The porous plasmonic microtubes manifest a SERS enhancement factor as high as 1×10^{10}, with only one order of variation along their lengths, indicating their good Raman response homogeneity.

METHODS

Synthesis of Au Nanoparticles Using D-Glucose as Reducing and Stabilizing Agent. Au nanoparticles (NPs) were synthesized in deionized (DI) water (ρ > 18.2 MΩ.cm), using chloroauric acid ($HAuCl_4 \cdot 3H_2O$, Sigma-Aldrich) as gold precursor, and D (dextro)-glucose ($C_6H_{12}O_6$, Omnichem) as reducing and stabilizing agent. Briefly, 30 mg of D-glucose (DG) was dissolved in 15 mL of DI water and then 0.5 mL of aqueous solution of gold ions (5 mM) was added. Finally, the pH of the solution was adjusted to 8.0 using a reference buffer solution of pH 10 (HNa_2O_4P, Sigma-Aldrich). The reduction of Au^{3+} ions and formation of gold nanoparticles were monitored recording the absorption spectra of the reaction mixture at different intervals, utilizing a SHIMADZU UV3100PC double beam spectrophotometer. A drop of colloid sample was dispersed over carbon-coated Cu grid for observations in scanning electron microscope SEM, ZEISS Auriga 3916) and transmission electron microscope (JEOL 2010F).

Inoculation of Fungi in Colloidal Gold Solution and Separation of the Gold-Coated Hyphae. Trichoderma asperelum (*T. asperelum*) and Aspergillus sydowii (*A. sydowii*) spores were inoculated in 5 mL of the previously prepared colloidal Au solution and stored in dark at room temperature. The growth of fungi in the colloidal solution was noted after 8 days. After 12 days, a part of the grown mycelium was taken out, redispersed in water, and washed by repeated centrifugation (8 times at 1000 rpm for 5 min). The gold-coated hybrid structures were dispersed over glass and/or silicon substrates, and dried at room temperature for optical microscopic (ZEISS) and scanning electron microscopic (SEM, ZEISS Auriga 3916) observations.

Extraction of Organic Material from Hybrid Structures. The gold nanoparticle incorporated hybrid structures were placed over Si substrates simply by tweezer picking from their water dispersion. After drying in air (about 6 h, at room temperature), they were subjected to thermal treatment for removing the organic materials (including DG) from the hybrid structures. For this purpose, the samples were placed inside of an enclosed tubular Carbolite furnace, and heated to 400 °C under Ar flow (130 mL/min). On reaching this temperature, the Ar flow was stopped, and the temperature of the furnace was raised further to 520 °C (at 3 °C/min heating rate) under oxygen (130 mL/min) and argon (130 mL/min) gas mixture flow. After maintaining the sample temperature at 520 °C for 3 h, the furnace was cooled down to room temperature naturally. While the first step of thermal treatment was performed to transform the organic substances present in the hybrid to carbon through thermal pyrolysis, the second step was performed to eliminate most of the carbon from the gold microstructures through oxidation ($C + O_2 = CO_2\uparrow$).

Micro-Raman and SERS Study of Au Microtubes. A HORIBA Jobin Yvon HR800 microRaman system fitted with a charged couple device was used to record the Raman and SERS signals of selected analytes such as methylene blue (MB), rhodamine 6G (R6G), methyl orange (MO), and D-glucose (DG). The 632.8 nm line of a He−Ne laser was used for sample excitation. For Raman and SERS study, one drop (50 μL) of the aqueous analyte solution (15.6 μM concentration of MB, 10.5 μM concentration of R6G, 15.3 μM concentration of MO, and 25 mM concentration of DG) was dispersed over the Si substrate containing Au microtubes. For recording Raman and SERS signals, the exciting laser beam (He−Ne laser, λ = 632.8 nm, ∼50.0 μm spot size) was focused on the analyte droplet lying over bare Si substrate and gold microstructure over Si substrate, respectively.

Calculation of the SERS Signal Enhancement Factor. The SERS signal amplification, or enhancement factor (EF) was calculated following the procedure reported earlier,[33−35] utilizing the relation:

$$\mathrm{EF} = \frac{I_{\mathrm{SERS}} N_{\mathrm{RAMAN}}}{I_{\mathrm{RAMAN}} N_{\mathrm{SERS}}}$$

where I_{SERS} and I_{RAMAN} are the intensities of the same Raman band in the SERS and normal Raman spectrum, respectively. While N_{SERS} is the number of molecules adsorbed over the SERS substrate under excitation (under the exciting laser spot), N_{RAMAN} is the number of analyte molecules participated in normal Raman scattering. The parameters defining N_{SERS} and N_{RAMAN} are discussed in section S2 of the Supporting Information, along with the details of the EF calculation.

FDTD Calculations. Optical response and near-field enhancements in porous gold microtubes were calculated using the FDTD method, as implemented in the free software package MEEP.[36] In this method, Maxwell equations are solved by a second-order approximation. The space was divided into a discrete grid, the Yee grid,[37] and the evolution of the electric and magnetic fields was followed using discrete time steps. A schematic representation of the geometry used for the calculation is shown in Figure S7. A rough tubular structure of 1.0 μm diameter and 150 nm thickness was formed using a large number (n) of randomly distributed small Au spheres of 20−25 nm diameters. The numbers of Au particles considered for the construction microstructures were 5000 and 15 000, which correspond to filling fractions (ratio between the volume occupied by the spheres (Au NPs) and the total volume of the microtubes) of 0.5 and 0.9, respectively. The morphology of the final microstructures was very similar to that of the microstructures obtained by biotemplating in the present work. Because the constructed microtubes have high aspect ratios, we considered only their 1.0 μm sections for applying periodic boundary conditions in the direction parallel to the tube axis (i.e., an infinitely long cylinder). An infinite space was simulated in the other two spatial axes by applying perfectly matched layers. The dimensions of the constructed microtubes were intentionally kept smaller than the dimensions of the experimentally obtained microtubes to improve the speed of the calculations. The results obtained from calculation are considered accurate and representative because the intensity of the "hot spots" is controlled by the surface roughness of the tubular structures rather than their diameter. Simulations were performed for the polarizations parallel and perpendicular to the tube axis. In all calculations, we used a spatial resolution of ∼10 nm.

RESULTS AND DISCUSSION

Utilizing nonpathogenic filamentous fungi such as *T. asperellum* and *A. sydowii* as living templates, we synthesized gold microtubes of diameters in-between 2.0 and 4.0 μm, and several micrometres in length. The fabrication process involved the incorporation of prefabricated Au nanoparticles (NPs) into

DOI: 10.1021/acsanm.9b00443
ACS Appl. Nano Mater. 2019, 2, 2533−2541

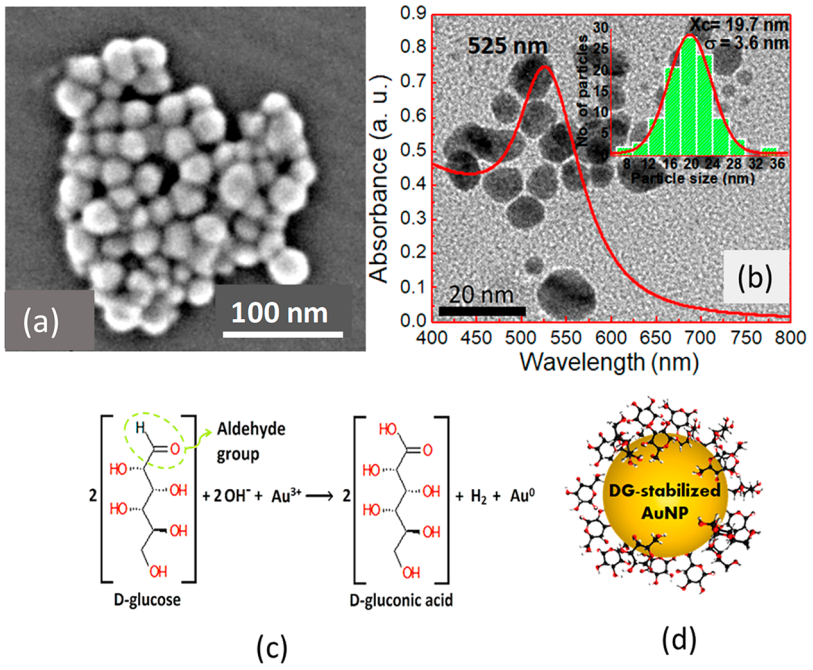

Figure 1. Typical (a) SEM and (b) TEM micrographs of Au nanoparticles fabricated by DG reduction of Au^{3+} ions. The inset in b shows the absorption spectrum of the colloidal gold nanoparticles and their size distribution histogram. The mechanism of (c) gold ion (Au^{3+}) reduction and (d) formation of glucose stabilized gold nanoparticles. Reduction of gold ion (Au^{3+}) occurs through the electron transfer from oxygen atom of the aldehyde group of DG to gold ions, oxidizing DG and producing D-gluconic acid. The OH groups of the D-gluconic acid get attached to the surface of Au NPs through electrostatic interaction, providing their stability.[38] The black, red, and white spheres in d are the C, O, and H atoms, respectively.

the cell walls of the fungi and careful elimination of biological templates. First, Au nanoparticles of about 20 nm average size were fabricated using D-glucose (DG) both as reducing and stabilizing agent (Figure 1).

T. asperellum and *A. sydowii* spores were inoculated in the colloidal gold solution. In about 8 days, fungal hyphae were grown in Au colloid solution (Figure 2). Figure 3a–c shows

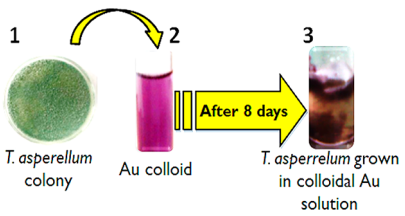

Figure 2. Schematic illustration of the inoculation of fungus spores in the Au colloid medium and growth of fungus. The growth of fungus was observed after 8 days of inoculation. The DG in the colloidal medium acts as nutrient for the growth of fungus.

typical optical microscopy images of *T. asperellum* hyphae grown in aqueous DG solutions. As can be seen from Figure 3b, c, the fungal hyphae grown in Au colloid become dark, due to the adhesion of Au NPs on their cell walls. Uniform coverage of fungal hyphae by the Au NPs could be further verified from the scanning electron microscopy (SEM) image and elemental mapping of the Au NP-covered hyphae presented in Figure 3d.

The tubular hyphae of the filamentous fungi used as templates consist of cell walls of 80–400 nm thickness, plasma membrane of about 10 nm thickness, and cytoplasm. The plasma membrane, located beneath the cell wall, protects the cytoplasm and controls the transport of nutrients. The cell wall, which is in direct contact with the surrounding medium, provides protection and mechanical strength along with flexibility to the hypha. It composed predominantly of polysaccharides such as chitin, mannans, glucans, and transiting proteins. Chitin forms the inner layer of the cell wall with a quasi-ordered (fibrillary) structure, whereas mannans, glucans, and transiting proteins form the outer amorphous layer (Figure 4a).[39,40] The outer layer of the cell wall contains pores of a few nanometers in diameter. Depending on the growth phase of the fungi and the vegetative stress, the diameter of these pores can vary from 30 to 200 nm.[41,42] The colloidal gold NPs in random motion introduce into these pores of fungus cell wall and get attached to it through intermolecular hydrogen bonding between the OH groups of nanoparticle-bonded glucose molecules and OH groups of polysaccharides (chitin, glucans, and mannans) of the cell wall as demonstrated in Figure S2. The processes involved in the attachment and assembly of Au NPs over the cell wall of fungal hyphae are presented schematically in Figure 4.

After collecting the Au nanoparticle-covered hyphae from their growth solution (Figure 2) and washing in water, they were subjected to a two-step thermal treatment process under controlled ambient; first to transform all the organic substances (including the biotemplate and DG) to carbon, and then to eliminate a major portion of the formed carbon and partial fusion of Au NPs to form Au microtubes. During the heat treatment of the hybrid (organic–inorganic; Au NP assembled fungal hyphae) structures, apat from removing the organic substances, a partial fusion of Au NPs occurred, which helped them to interconnect and fabricate porous Au microtubes. As can be noticed from the SEM micrographs provided in Figure

DOI: 10.1021/acsanm.9b00443
ACS Appl. Nano Mater. 2019, 2, 2533–2541

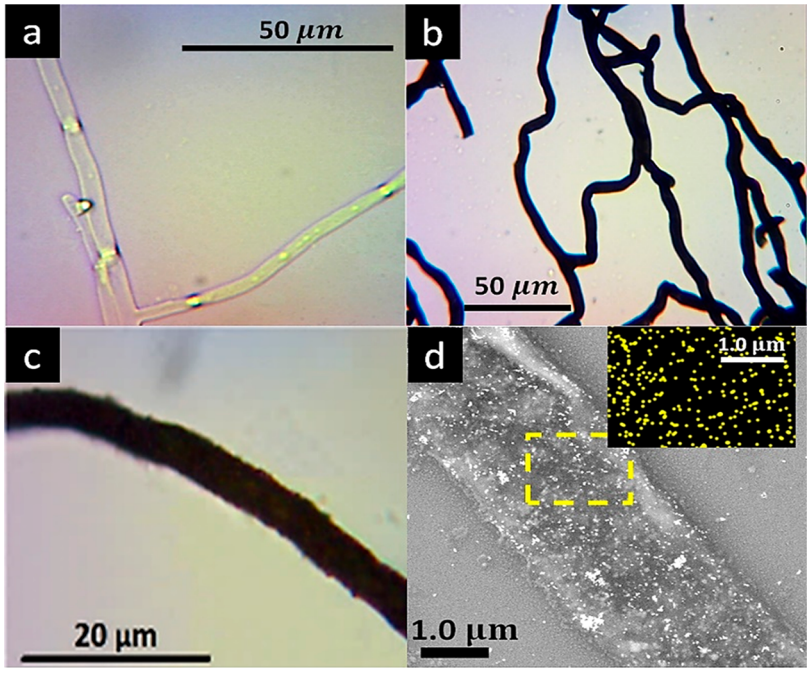

Figure 3. Typical optical microscopic images of *T. asperellum* hyphae grown in (a) aqueous DG solution (without Au NPs), and in (b, c) Au NP containing colloid medium (after 12 days of inoculation). Typical SEM image of a nanoparticle-attached *T. asperellum* hypha and EDS elemental Au mapping at its selected region (marked by yellow square) are presented in (d) showing the uniform attachment of Au NPs at the surface of fungal hyphae.

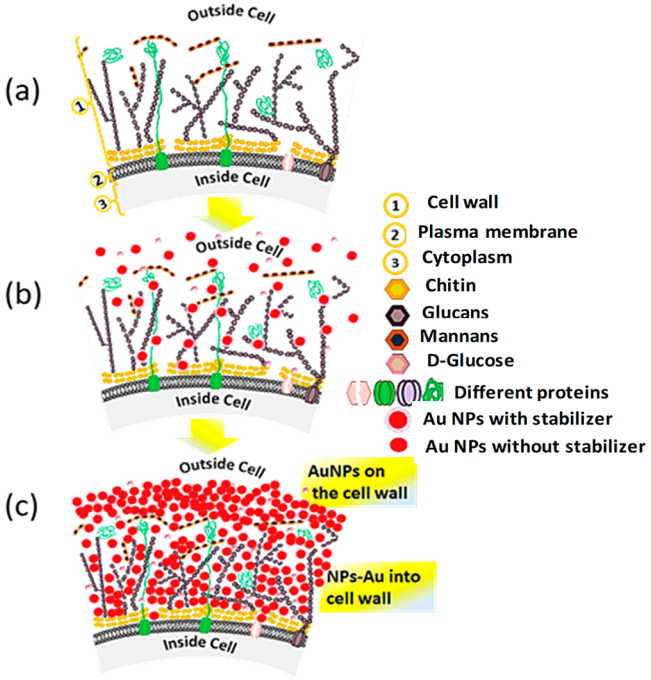

Figure 4. Schematic presentation of Au nanoparticle self-assembly process in hypha cell wall: (a) The porous cell wall composed of mannans, glucans, chitin and transiting proteins;[34] (b) introduction of Au NPs into cell wall pores and attachment through intermolecular hydrogen bonding; (c) attachment and agglomeration of Au NPs with the cell wall, leading to their assembly over the cell wall of the fungus hyphae.

5, the Au NPs are not completely fused/melted, and the Au microstructures have porous, corrugated surfaces. While the two-step annealing process used in the present work is pretty simple and easy to implement, the process of fabrication of Au microtubes through this annealing process is fully reproducible.

The gold microtubes thermally extracted from the organic templates are shown in Figure 5a–f. As can be seen in the images of Figure 5, the microstructures exhibit porous and corrugated surface, which make them ideal for utilization as SERS substrates. The formed microstructures of 8–60 μm length have an average wall thickness of about 180 nm, and diameter of 2–4 μm. Although the length of the fungi hyphae used as biotemplate can extend over tens of centimeters, the obtained gold microtubes are relatively shorter as the Au NP-coated hyphae were broken during the sonication process used during their cleaning (before thermal treatment). The tubular form of the obtained microstructures indicates the Au NPs (~20 nm average size) do not pass through the semipermeable cytoplasm membrane of the fungal hyphae.

Aqueous solutions containing methylene blue (MB), rhodamine 6G (R6G), methyl orange (MO), and D-glucose (DG) of concentrations 15.6, 10.5, and 15.3 μM and 25 mM, respectively, were used for SERS tests. Raman spectra were recorded by exposing the laser beam on the analyte droplet placed over the plasmoic microstructure and outside (i.e., over the Si substrate). The analyte solution droplet placed over the gold microtube was not dried before the measurements. Although several procedures have been adapted by the researchers for recording SERS spectra of analytes, the procedure we followed in this work is the one reported by Yang et al.[8]

When a drop of each of these aqueous solutions was placed on a bare silicon substrate, no detectable signal was observed apart from the transverse optical (TO) phonon mode of silicon on exciting with a He–Ne laser (λ = 632.8 nm, 10 mW, 1.0 mm spot size) (Figure 6a). On the other hand, when a drop of each of these solutions was placed on single Au microtube, SERS signals of the analyte molecules were obtained at high

DOI: 10.1021/acsanm.9b00443
ACS Appl. Nano Mater. 2019, 2, 2533–2541

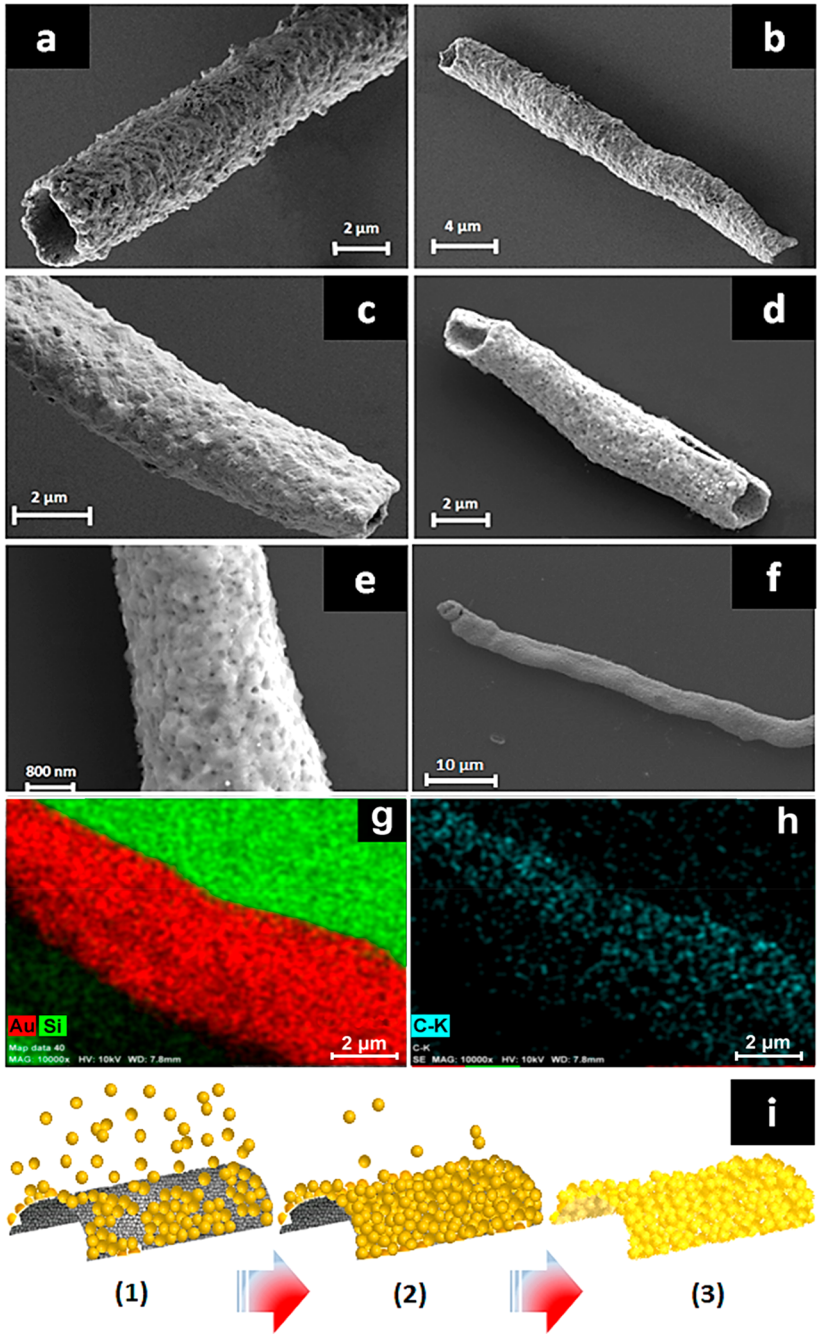

Figure 5. (a–f) Typical SEM images of tubular Au microstructure obtained after removing organic template. The porous and corrugated nature of the microstructure surface formed by interconnected Au NPs can be perceived from the amplified images presented in c and e. (g, h) Elemental mapping over a section of an Au microtube, showing uniform distribution of Au and carbon. (i) Schematic illustration of the steps utilized for the (1) attachment and assembly of colloidal Au NPs (golden spheres) over hyphae cell wall (porous mesh in gray), (2) agglomeration of Au NPs over the cell wall of the hypha, and (3) Au microtube formed by interconnected Au NPs after removing organic template.

intensities (about a thousand times more intense than those recorded without Au microtubes) (Figure 6b).

Figure 7 shows the normal Raman and SERS spectra of each of the used analytes. As can be noted, the SERS responses of MB and R6G are much higher than of MO and DG molecules. In the case of R6G molecule, the normal Raman cross-section is larger than those of the MB, MO, and DG molecules. However, in the case of the MB molecule, as its absorption wavelength (around 650 nm) is close to the laser excitation wavelength,[43] i.e., close to the resonance, intensity of the SERS signal was higher. On the other hand, DG molecules revealed the lowest SERS response because of their smallest Raman cross-section. Although the SERS signal intensity is about 12 000 times higher than the Raman signal for R6G molecules, it is about 3000 times higher for DG molecules.

Because of the relaxation of selection rules,[44] all the analyte molecules revealed a large number of vibrational modes (Figure S3 and Tables S2, S3, S4, and S5). Most of the SERS signals of the analytes were shifted from their reported normal Raman peak positions, indicating that they are chemisorbed on the surface of the Au microtubes.[45]

DOI: 10.1021/acsanm.9b00443
ACS Appl. Nano Mater. 2019, 2, 2533–2541

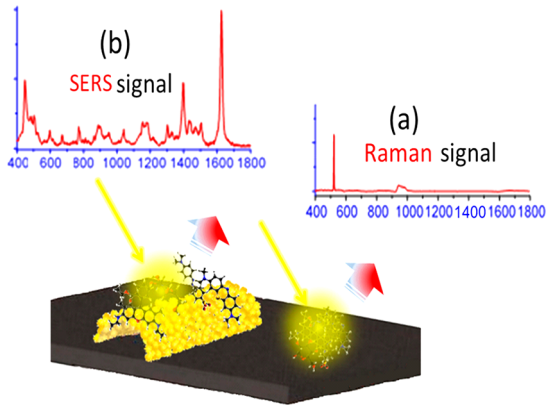

Figure 6. Schematic presentation of the measurements performed for recording the normal Raman and SERS spectra of the analytes: (a) analytes located over the bare silicon substrate revealing the TO band of the Si substrate; (b) analytes located over the Au microstructure producing SERS signals.

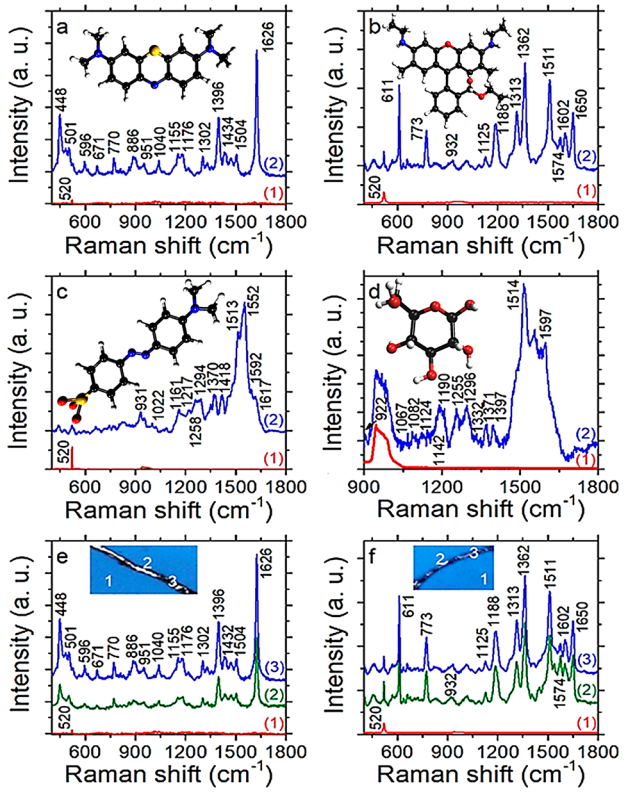

Figure 7. Characteristic Raman (line 1, red color) and SERS (lines 2 and 3, in green and blue color, repectively) spectra of target molecules: (a) MB (15.6 μm), (b) R6G (10.5 μm), (c) MO (15.3 μm), and (d) DG (25 mM).

SERS spectra of the analyte solutions over a gold microtube revealed characteristic bands associated with the vibrational modes of analyte molecules (Supporting Information Section 3). Raman spectra of the analyte molecules measured by dispersing their solutions over silicon wafer (without gold microstructures) revealed mainly the characteristic 520 cm^{-1} band associated with the fundamental TO mode of bulk silicon at Γ-point. Raman and SERS signals of (e) R6G and (f) MO solutions acquired at different positions (inset optical images) of the tubular Au microstructures revealed higher SERS signal at the denser parts of the microstructures. However, maximum variation of SERS signal intensity along the microstructure length was only 1 order of magnitude.

For the calculation of average SERS enhancement factors (EFs), the I_{SERS}/I_{RAMAN} ratios for MB, R6G, MO, and DG were estimated considering their most prominent Raman signals located at 1626, 1362, 1552, and 1514 cm^{-1}, respectively. The bands were fitted to Lorentzian distribution curves, and the areas under the curves were considered as their intensities. For the calculation of N_{NR}/N_{SERS} ratio, parameters such as laser spot size, analyte concentration, laser-penetration depth, substrate surface area, drop-volume of the analyte, density, and molecular mass of the analyte molecules were considered. Details of the EF calculation is supplied in the Supporting Information (Section S2). SERS enhancement factors calculated for the MB, R6G, MO, and DG analytes were 1.19 × 10^{10}, 8.89 × 10^{9}, 7.84 × 10^{9}, and 5.47 × 10^{6}, respectively. As can be noted, the highest EF was attained for MB and the lowest for DG. As has been discussed earlier, the drastic (four-order) difference between the EFs of MB and DG is due to the differences in their normal Raman cross-sections and the proximity of the excitation (laser beam) wavelength to the corresponding Raman signals of MB. The high EF values obtained for the analytes indicate the presence of intense local electric field (hot spots) at the surface of microstructures. Most of the estimated EF values are well above the single-molecule detection limit, which is ∼1 × 10^{7} for Plasmonic SERS substrates.[46−5053] Although higher SERS enhancement factors have been reported for plasmonic nanostructures self-assembled over analyte layers in the literature,[51] the substrates are analyte specific.

In comparison to the Au microtubes fabricated using *T. asperellum*, Au microtubes obtained using *A. sydowii* as template were of slightly smaller diameters (1.5−3.0 μm, not presented). However, the SERS responses of the latter microtubes were seen to be very similar (not presented) to the former microtubes (fabricated using *T. asperellum*) for all the analytes tested in the present study.

As the homogeneity of plasmonic substrates is one of the principal impediments and a mejor issue for utilizing them in SERS based molecular detection, we studied the SERS response of a few of the fabricated Au microtubes along their lengths, which revealed only 1 order of variation in SERS intensity. Moreover, contrary to the conventional SERS substrates, we do not need to assemble these Au microtubes for utilization as SERS substrate. In fact, each of the Au microtubes of the present study can work as individual SERS substrate.

To verify the SERS response homogeneity of the Au microtubes, we recorded the SERS signals at the denser (higher Au density) and of the sparser (low Au density) regions of the microstructures for all the tested analytes. As can be noticed from Figure 7e, f, the tubular Au microstructures reveal higher SERS signal at the denser parts than the sparser parts. However, the maximum variation in SERS signal intensity recorded along the microstructure length was only 1 order of magnitude, which probably occurred because of the variation in local electric field intensity because the assembly of the Au NPs along the microstructures is not homogeneous (Figures S4 and S5). Although an exact calculation of EF considering the variations of adsorbed analyte molecules is almost impossible, the observed one-order EF variation along the microstructures indicates their consistent signal response,

DOI: 10.1021/acsanm.9b00443
ACS Appl. Nano Mater. 2019, 2, 2533−2541

making them promising for applications such as SERS-based biosensors.

To test the detection sensitivity of the plasmonic microtubes, we recorded SERS spectra of MB (the analyte with highest estimated EF) solutions of different concentrations over a single Au microtube. In fact, the procedure was repeated over 4 different microtubes to estimate the average SERS response of the Au microtubes for different MB concentrations. As can be seen from Figure S6, the variation of SERS signal (average) intensity for a wide concentration range (0.01 to 3.12 μM) of MB is almost linear. The minimum detectable concentration was 10 nM.

To highlight the effect of compactness of the Au NPs on the SERS response of the microtubes, we performed electromagnetic calculations using the finite-deference time-domain (FDTD) method as implemented in the free software MEEP (Figure S7).[36] In particular, we explored the dependence of the near-field intensity as the function of surface roughness of the microtube, excitation conditions (polarization of light) and exciting wavelength. Near-field enhancements calculated for some selected structures are presented in Figures 8a–d. As can be seen, remarkable field enhancement can be obtained for both sparse (filling fraction = 0.5) and dense (filling fraction = 0.9) microtubes, far larger than the field enhancement ($|\mathbf{E}|^4/|\mathbf{E}_0|^4 \approx 16$, blue horizontal dashed line in Figure 8e) produced in a perfect microtube (filling fraction = 1). It is interesting to note that the field enhancement in such porous microtubes is expanded through a wider spectral range. The wide band near-field effect can be followed in Figure 8e, where the field enhancement is plotted as a function of excitation wavelength for the two considered microstructures. As can be noted, field enhancement for the microtube with filling fraction 0.5 is spanned over 850–1050 nm, with maximum located around 870 nm. For the microstructure with filling fraction 0.9, the field enhancement spanned over 600–750 nm, with a maximum located around 660 nm. From the theoretical results presented in Figure 8, it seems the Au microtubes fabricated by our fungal hyphae template method closely resemble the characteristics of the microtubules with filling fraction 0.9. The field enhancement over wide spectral range makes these microstructures efficient SERS substrates for a wide range of excitation wavelengths.

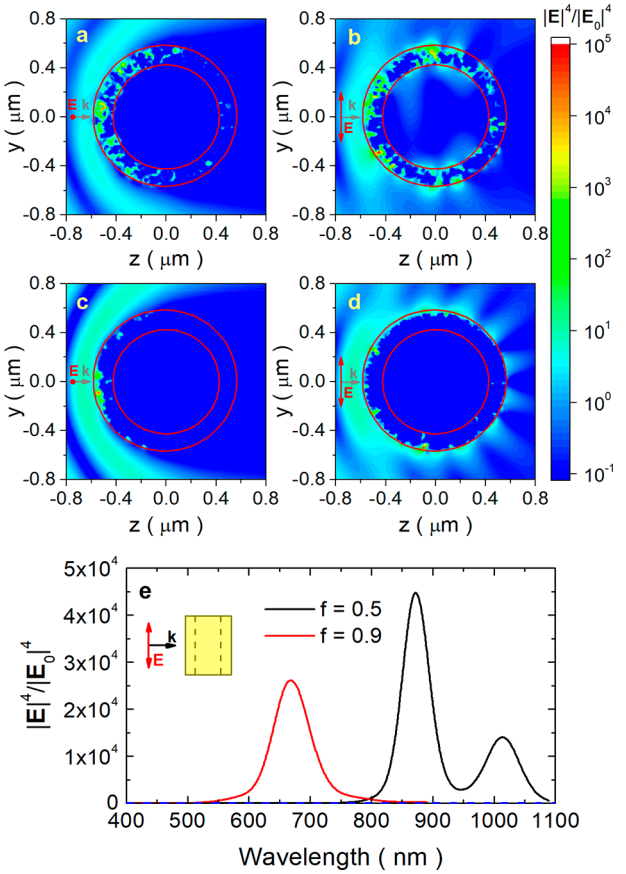

Figure 8. Transversal near-field color maps for two different gold microtubes with filling fractions of (a b) 0.5 and (c, d) 0.9. For all cases, a plane wave is propagating from left to right with polarization either (a, c) parallel or (b,d) perpendicular to the axis of the microtube. The wavelength of the incident bean is 870 nm, and 680 nm for the filling fraction of 0.5 and 0.9, respectively. (e) Maximum field enhancement as a function of wavelength for two gold microtubes with filling fractions of 0.5 and 0.9. Field enhancement for a perfect microtube is shown as blue horizontal dashed lines for reference.

Although the enhancement of Raman signal by plasmonic substrates is generally governed through near-field enhancement around plasmonic NPs, the position and intensity of SERS signals depend on the nature of bonding of analyte molecules with substrate.[52,53] Spectral shifts observed for the Raman signals of our tested analytes indicate that apart from the electromagnetic effects on the analyte molecules physisorbed over Au surface, chemical effects are also active. Presence of carbon impregnated into the Au microtubes is believed to induce chemisorption of analyte molecules at their surface.[53]

CONCLUSIONS

The results obtained in this study demonstrate that it is possible to fabricate tubular Au microstructures with a porous and corrugated surface in large quantities (a few thousand in a single synthesis process) using nonpathogenic filamentous fungi such as *T. asperellum* and *S. sydowii* as organic templates and an organic reducer such as DG. Controlling the conditions of thermal annealing, it is possible to incorporate (impregnate) carbon nanoparticles into the porous wall of Au microtubes. The presence of carbon in the microstructures increases their SERS enhancement ability through chemisorption of analyte molecules. The high SERS enhancement ability and only one order variation of EF along their length make these Au microstructures promising material for developing highly sensitive molecular sensors at low cost. Moreover, the Au microtubes can be fabricated by completely green processing techniques.

ASSOCIATED CONTENT

Supporting Information

The Supporting Information is available free of charge on the ACS Publications website at DOI: 10.1021/acsanm.9b00443.

Calculation of SERS enhancement factor (EF); hydrogen bond formation between Au nanoparticle-bound D-glucose or D-gluconic acid and the cell wall constituents; vibrational modes and Raman shift (band assignment) for MB, R6G, MO, and DG; sensibility of Au microtubes as SERS-based molecular sensors; and FDTD calculations (PDF)

DOI: 10.1021/acsanm.9b00443
ACS Appl. Nano Mater. 2019, 2, 2533–2541

AUTHOR INFORMATION

Corresponding Author

*E-mail: upal@ifuap.buap.mx (U.P.).

ORCID

Umapada Pal: 0000-0002-5665-106X

Ovidio Peña-Rodríguez: 0000-0002-7329-0550

Present Address

‡D.N.C.L. is currently at the Facultad de Ciencias Electronicas, Benemérita Universidad Autónoma de Puebla.

Notes

The authors declare no competing financial interest.

REFERENCES

(1) Xia, Y.; Xiong, Y.; Lim, B.; Skrabalak, S. E. Shape-controlled Synthesis of Metal Nanocrystals: Simple Chemistry Meets Complex Physics? *Angew. Chem., Int. Ed.* **2009**, *48*, 60−103.

(2) Bell, S. E. J.; Sirimuthu, N. M. S. Quantitative Surface-enhanced Raman Spectroscopy. *Chem. Soc. Rev.* **2008**, *37*, 1012−1024.

(3) Reilly, T. H.; Chang, S.-H.; Corbman, J. D.; Schatz, G. C.; Rowlen, K. L. Quantitative Evaluation of Plasmon Enhanced Raman Scattering from Nanoaperture Arrays. *J. Phys. Chem. C* **2007**, *111*, 1689−1694.

(4) Hailin, X.; Leiming, W.; Xiaoyu, D.; Yanxia, G.; Yuanjiang, X. An Ultra-high Sensitivity Surface Plasmon Resonance Sensor based on Graphene-Aluminum-Graphene Sandwich-like Structure. *J. Appl. Phys.* **2016**, *120*, No. 053101.

(5) Zhang, Z.; Yang, J.; He, X.; Zhang, J.; Huang, J.; Chen, D.; Han, Y. Plasmonic Refractive Index Sensor with High Figure of Merit based on Concentric-Rings Resonator. *Sensors* **2018**, *18*, 116.

(6) Ding, Y.; Zhang, X.; Yin, H.; Meng, Q.; Zhao, Y.; Liu, L.; Wu, Z.; Xu, H. Quantitative and Sensitive Detection of Chloramphenicol by Surface-Enhanced Raman Scattering. *Sensors* **2017**, *17*, 2962.

(7) Anker, J. N.; Paige, W.; Lyandres, H. O.; Shah, N. C.; Zhao, J.; Van Duyne, R. P. Biosensing with Plasmonic Nanosensors. *Nat. Mater.* **2008**, *7*, 442−453.

(8) Yang, S.; Dai, X.; Stogin, B. B.; Wong, T.-S. Ultrasensitive Surface-Enhanced Raman Scattering Detection in Common Fluids. *Proc. Natl. Acad. Sci. U. S. A.* **2016**, *113*, 268−273.

(9) Fleischmann, M.; Hendra, P. J.; McQuillan, A. J. Raman Spectra of Pyridine adsorbed at a Silver Electrode. *Chem. Phys. Lett.* **1974**, *26*, 163−166.

(10) Moskovits, M. Surface-Enhanced Raman Spectroscopy: A Brief Perspective. In *Surface-Enhanced Raman Scattering*; Kneipp, K., Moskovits, M., Kneipp, H., Eds.; Springer: Berlin, 2006; pp 1−17. DOI: 10.1007/3-540-33567-6_1

(11) Jackson, J. B.; Halas, N. J. Surface-Enhanced Raman Scattering on Tunable Plasmonic Nanoparticle Substrates. *Proc. Natl. Acad. Sci. U. S. A.* **2004**, *101*, 17930−17935.

(12) Chakraborty, I.; Bag, S.; Landman, U.; Pradeep, T. Atomically precise Silver Clusters as new SERS Substrates. *J. Phys. Chem. Lett.* **2013**, *4*, 2769−2773.

(13) Ferchichi, A.; Laariedh, F.; Sow, I.; Gourgon, C.; Boussey, J. Fabrication of Disposable Flexible SERS Substrates by Nanoimprint. *Microelectron. Eng.* **2015**, *140*, 52−55.

(14) Abu Hatab, N. A.; Oran, J. M.; Sepaniak, M. J. Surface-Enhanced Raman Spectroscopy Substrates created via Electron Beam Lithography and Nanotransfer Printing. *ACS Nano* **2008**, *2*, 377−385.

(15) Zhang, Q.; Li, W.; Moran, C.; Zeng, J.; Chen, J.; Wen, L.-P.; Xia, Y. Seed-mediated Synthesis of Ag Nanocubes with Controllable Edge Lengths in the range of 30−200 nm and Comparison of their Optical Properties. *J. Am. Chem. Soc.* **2010**, *132*, 11372−11378.

(16) Freeman, R. G.; Grabar, K. C.; Allison, K. J.; Bright, R. M.; Davis, J. A.; Guthrie, A. P.; Hommer, M. B.; Jackson, M. A.; Smith, P. C.; Walter, D. G.; Natan, M. J. Self-Assembled Metal Colloid Monolayers: An approach to SERS Substrates. *Science* **1995**, *267*, 1629−1632.

(17) Greeneltch, N. G.; Blaber, M. G.; Schatz, G. C.; Van Duyne, R. P. Plasmon-sampled Surface-Enhanced Raman Excitation Spectroscopy on Silver immobilized Nanorod Assemblies and Optimization for Near Infrared (λ_{ex} = 1064 nm) Studies. *J. Phys. Chem. C* **2013**, *117*, 2554−2558.

(18) Greeneltch, N. G.; Blaber, M. G.; Henry, A.-I.; Schatz, G. C.; Van Duyne, R. P. Immobilized Nanorod Assemblies: Fabrication and Understanding of Large area Surface-Enhanced Raman Spectroscopy Substrates. *Anal. Chem.* **2013**, *85*, 2297−2303.

(19) Cinel, N. A.; Cakmakyapan, S.; Butun, S.; Ertas, G.; Ozbay, E. E-Beam Lithography designed Substrates for Surface Enhanced Raman Spectroscopy. *Photonics Nanostructures - Fundam.Appl.* **2015**, *15*, 109−115.

(20) Fan, M.; Brolo, A. G. Silver Nanoparticles Self-assembly as SERS Substrates with near Single Molecule Detection Limit. *Phys. Chem. Chem. Phys.* **2009**, *11*, 7381−7389.

(21) McFarland, A. D.; Young, M. A.; Dieringer, J. A.; Van Duyne, R. P. Wavelength-Scanned Surface-Enhanced Raman Excitation Spectroscopy. *J. Phys. Chem. B* **2005**, *109*, 11279−11285.

(22) Zou, S.; Schatz, G. C. Silver Nanoparticle array Structures that Produce Giant Enhancements in Electromagnetic Fields. *Chem. Phys. Lett.* **2005**, *403*, 62−67.

(23) Sugunan, A.; Melin, P.; Schnürer, J.; Hilborn, J. G.; Dutta, J. Nutrition-driven Assembly of Colloidal Nanoparticles: Growing Fungi Assemble Gold Nanoparticles as Microwires. *Adv. Mater.* **2007**, *19*, 77−81.

(24) Dujardin, E.; Peet, C.; Stubbs, G.; Culver, J. N.; Mann, S. Organization of Metallic Nanoparticles using Tobacco Mosaic Virus Templates. *Nano Lett.* **2003**, *3*, 413−417.

(25) Li, Z.; Chung, S.-W.; Nam, J.-M.; Ginger, D. S.; Mirkin, C. A. Living Templates for the Hierarchical Assembly of Gold Nanoparticles. *Angew. Chem., Int. Ed.* **2003**, *42*, 2306−2309.

(26) Rehman, A.; Majeed, M. I.; Ihsan, A.; Hussain, S. Z.; Rehman, S.; Ghauri, M. A.; Hussain, I. Living Fungal Hyphae-templated Porous Gold Microwires using Nanoparticles as Building Blocks. *J. Nanopart. Res.* **2011**, *13*, 6747−6754.

(27) Sabah, A.; Dakua, I.; Kumar, P.; Mohammed, W. S.; Dutta, J. Growth of Templated Gold Microwires by Self-Organization of Colloids on *Aspergillus Niger*. *Dig. J. Nanomater. Biostructures* **2012**, *7*, 583−591.

(28) Berry, V.; Saraf, R. F. Self-assembly of Nanoparticles on Live Bacterium: An Avenue to Fabricate Electronic Devices. *Angew. Chem., Int. Ed.* **2005**, *44*, 6668−6673.

(29) Quester, K.; Avalos-Borja, M.; Vilchis-Nestor, A. R.; Camacho-López, M. A.; Castro-Longoria, E. SERS Properties of Different Sized and Shaped Gold Nanoparticles Biosynthesized under Different Environmental Conditions by *Neurospora Crassa* Extract. *PLoS One* **2013**, *8*, No. e77486.

(30) Coman, C.; Leopold, L. F.; Ruginǎ, O. D.; Barbu-Tudoran, L.; Leopold, N.; Tofanǎ, M.; Socaciu, C. Green Synthesis of Gold Nanoparticles by *Allium Sativum* Extract and their Assessment as SERS Substrate. *J. Nanopart. Res.* **2014**, *16*, 1−9.

(31) Liu, R.; Wei, Y.; Zheng, J.; Zhang, H.; Sheng, Q. A Hydrogen peroxide Sensor based on Silver Nanoparticles Biosynthesized by *BacillusSubtilis*. *Chin. J. Chem.* **2013**, *31*, 1519−1525.

(32) Yang, D. P.; Chen, S.; Huang, P.; Wang, X.; Jiang, W.; Pandoli, O.; Cui, D. Bacteria-Template Synthesized Silver Microspheres with Hollow and Porous Structures as Excellent SERS Substrate. *Green Chem.* **2010**, *12*, 2038−2042.

(33) Zhang, Q.; Li, X.; Ma, Q.; Zhang, Q.; Bai, H.; Yi, W.; Liu, J.; Han, J.; Xi, G. A Metallic Molybdenum dioxide with High Stability for Surface Enhanced Raman Spectroscopy. *Nat. Commun.* **2017**, *8*, 14903.

(34) Cong, S.; Yuan, Y.; Chen, Z.; Hou, J.; Yang, M.; Su, Y.; Zhang, Y.; Li, Q.; Geng, F.; Zhao, Z. Noble Metal-comparable SERS Enhancement from Semiconducting Metal Oxides by making Oxygen Vacancies. *Nat. Commun.* **2015**, *6*, 7800.

(35) Ben-Jaber, S.; Peveler, W. J.; Quesada-Cabrera, R.; Sol, C. W. O.; Papakonstantinou, I.; Parkin, I. P. Sensitive and Specific Detection

DOI: 10.1021/acsanm.9b00443
ACS Appl. Nano Mater. 2019, 2, 2533−2541

of Explosives in Solution and Vapour by Surface-Enhanced Raman Spectroscopy on Silver Nanocubes. *Nanoscale* **2017**, *9*, 16459.
(36) Oskooi, A. F.; Roundy, D.; lbanescu, M.; Bermel, P.; Joannopoulos, J. D.; Johnson, S. G. Meep: A Flexible free-software Package for Electromagnetic Simulations by the FDTD Method. *Comput. Phys. Commun.* **2010**, *181*, 687−702.
(37) Yee, K. Numerical Solution of initial Boundary Value Problems involving Maxwell's Equations in Isotropic Media. *IEEE Trans. Antennas Propag.* **1966**, *14*, 302−307.
(38) Castillo-López, D. N.; Pal, U. Green Synthesis of Au Nanoparticles using Potato Extract: Stability and Growth Mechanism. *J. Nanopart. Res.* **2014**, *16*, 1−15.
(39) Deacon, J.; *Fungal Biology*,4th ed.; Blackwell Publishing: Oxford, U.K., 2006.
(40) Moore-Landecker, E. *Fundamentals of the Fungi*; Cummings, B., Ed.; Prentice Hall, 1996.
(41) de Souza Pereira, R.; Geibel, J. Direct Observation of Oxidative Stress on the Cell Wall of *Saccharomyces Cerevisiae* Strains with Atomic Force Microscopy. *Mol. Cell. Biochem.* **1999**, *201*, 17−24.
(42) Casadevall, A.; Nosanchuk, J. D.; Williamson, P.; Rodrigues, M. L. Vesicular Transport across the Fungal Cell Wall. *Trends Microbiol.* **2009**, *17*, 158−162.
(43) Jacobs, K. Y.; Schoonheydt, R. A. Time Dependence of the Spectra of Methylene Blue-Clay Mineral Suspensions. *Langmuir* **2001**, *17*, 5150−5155.
(44) Moskovits, M.; Suh, J. S. Surface Selection Rules for Surface-Enhanced Raman Spectroscopy: Calculations and Application to the Surface-Enhanced Raman Spectrum of Phthalazine on Silver. *J. Phys. Chem.* **1984**, *88*, 5526−5530.
(45) Xiao, G.-N.; Man, S.-Q. Surface-Enhanced Raman Scattering of Methylene Blue adsorbed on Cap-shaped Silver Nanoparticles. *Chem. Phys. Lett.* **2007**, *447*, 305−309.
(46) Patra, P. P.; Chikkaraddy, R.; Tripathi, R. P. N.; Dasgupta, A.; Kumar, G. V. P. Plasmofluidic Single-Molecule Surface-Enhanced Raman Scattering from Dynamic Assembly of Plasmonic Nanoparticles. *Nat. Commun.* **2014**, *5*, 4357.
(47) Zrimsek, A. B.; Henry, A.-I.; Van Duyne, R. P. Single Molecule Surface-Enhanced Raman Spectroscopy without Nanogaps. *J. Phys. Chem. Lett.* **2013**, *4*, 3206−3210.
(48) Blackie, E. J.; Le Ru, E. C.; Etchegoin, P. G. Single-Molecule Surface-Enhanced Raman Spectroscopy of Nonresonant Molecules. *J. Am. Chem. Soc.* **2009**, *131*, 14466−14472.
(49) Nie, S.; Emory, S. R. Probing Single Molecules and Single Nanoparticles by Surface-Enhanced Raman Scattering. *Science* **1997**, *275*, 1102−1106.
(50) Le Ru, E. C.; Meyer, M.; Etchegoin, P. G. Proof of Single-Molecule Sensitivity in Surface Enhanced Raman Scattering (SERS) by means of a Two-Analyte Technique. *J. Phys. Chem. B* **2006**, *110*, 1944−1948.
(51) Sisco, P. N.; Murphy, C. J. Surface-Coverage Dependence of Surface-Enhanced Raman Scattering from Gold Nanocubes on Self-Assembled Monolayers of Analyte. *J. Phys. Chem. A* **2009**, *113*, 3973−3978.
(52) Prakash, J.; Kumar, V.; Kroon, R. E.; Asokan, K.; Rigato, V.; Chae, K. H.; Gautam, S.; Swart, H. C. Optical and Surface Enhanced Raman Scattering properties of Au Nanoparticles Embedded in and Located on a Carbonaceous Matrix. *Phys. Chem. Chem. Phys.* **2016**, *18*, 2468−2480.
(53) Rout, C. S.; Kumar, A.; Fisher, T. S. Carbon Nanowalls Amplify the Surface-Enhanced Raman Scattering from Ag Nanoparticles. *Nanotechnology* **2011**, *22*, 395704.

DOI: 10.1021/acsanm.9b00443
ACS Appl. Nano Mater. 2019, 2, 2533−2541